Jung *et al. Energy Mater.* **2025**, *5*, 500118
DOI: 10.20517/energymater.2025.29

Energy Materials

Review

Open Access

Check for updates

Lithium manganese iron phosphate ($LiMn_{1-y}Fe_yPO_4$) rechargeable batteries: bridging material innovation with practical cell design

Heechul Jung[1], Chungsun Oh[1], Soyeon Park[1], Sieun An[1], Jeuk Bang[1], Jiyoung Youn[1], Jonghun Lee[1], Jun-Ho Park[2,3], Dongwook Han[1,*]

[1]Department of Future Energy Convergence, Seoul National University of Science and Technology, Seoul 01811, Republic of Korea.
[2]Battery Materials and Process Research Center, Battery Research Division, Korea Electrotechnology Research Institute (KERI), Changwon 51543, Republic of Korea.
[3]Department of Electro-Functionality Materials Engineering, University of Science and Technology (UST), Daejeon 34113, Republic of Korea.

***Correspondence to:** Prof. Dongwook Han, Department of Future Energy Convergence, Seoul National University of Science and Technology, 232 Gongneung-ro, Nowon-gu, Seoul 01811, Republic of Korea. E-mail: dw.han@seoultech.ac.kr

How to cite this article: Jung, H.; Oh, C.; Park, S.; An, S.; Bang, J.; Youn, J.; Lee, J.; Park, J. H.; Han, D. Lithium manganese iron phosphate ($LiMn_{1-y}Fe_yPO_4$) rechargeable batteries: bridging material innovation with practical cell design. *Energy Mater.* **2025**, *5*, 500118. https://dx.doi.org/10.20517/energymater.2025.29

Received: 1 Feb 2025 **First Decision:** 1 Apr 2025 **Revised:** 15 Apr 2025 **Accepted:** 30 Apr 2025 **Published:** 10 Jun 2025

Academic Editor: Meicheng Li **Copy Editor:** Fangling Lan **Production Editor:** Fangling Lan

Abstract

The growing demand for high-energy storage, rapid power delivery, and excellent safety in contemporary Li-ion rechargeable batteries (LIBs) has driven extensive research into lithium manganese iron phosphates ($LiMn_{1-y}Fe_yPO_4$, LMFP) as promising cathode materials. The strong P-O covalent bonds in the olivine structure of LMFP ensure exceptional thermal and structural stability compared to conventional layered $LiNi_{1-y-z}Co_yMn_zO_2$ (NCM). In addition, the relatively low energy density of $LiFePO_4$ (LFP), which is isostructural to LMFP, has been significantly increased by the incorporation of Mn redox reactions with a strong reducing tendency. This widespread recognition has advanced our understanding of the physicochemical characteristics of LMFP, which are closely related to its chemical compositions, particle morphology, synthesis processes, and cycling conditions. Despite notable progress in improving the structural integrity and electrochemical superiority of LMFP, most academic research has focused on LMFP/lithium metal half-cell systems. However, practical applications of LIBs require more intricate system configurations involving non-Li anode materials, such as graphite and $Li_4Ti_5O_{12}$ (LTO). This comprehensive review explores key electrochemical phenomena in LMFP/graphite and LMFP/LTO full cells under both standard and elevated temperatures. Additionally, it offers insights into optimal cell design strategies

and practical technologies aimed at achieving a well-balanced combination of energy density, thermal stability, and cost-effectiveness. These advancements position LMFP-based rechargeable batteries as a promising solution for next-generation energy storage systems.

Keywords: Lithium manganese iron phosphates, graphite, lithium titanate, cell design optimization, practical technologies, lithium-ion rechargeable batteries

INTRODUCTION

Since 1991, advancements in Li-ion rechargeable batteries (LIBs), which provide intermittent power to electric devices as needed, have driven societal progress[1]. However, current LIBs face increasing challenges related to sustainability and safety due to the scarcity of rare-earth elements (Co and Ni) and the limited structural and thermal stability of cathode materials[2]. As a result, the dominance of conventional layered $LiNi_{1-y-z}Co_yMn_zO_2$ (NCM) is being challenged, leading to a gradual shift to olivine $LiFePO_4$ (LFP) and $LiMn_{1-y}Fe_yPO_4$ (LMFP) cathode materials[3,4]. The structural integrity and extended cycle life of olivine L(M)FP, supported by strong P-O covalent bonds, have been demonstrated even under high current densities and extreme environmental conditions. Additionally, the widespread availability of its key transition metals (Fe and Mn) in the Earth's crust significantly reduces production costs. Despite these advantages, the tap density and low-temperature performance of L(M)FP are inferior to those of the NCM materials[3,5]. In this context, it is imperative to comprehensively consider energy density, temperature-dependent reaction kinetics, cycle life, safety, sustainability, and cost across multiple scales, including the particle, electrode, cell, and pack levels, when engineering optimal cathode materials.

The theoretical gravimetric energy density (~578 W h kg^{-1}) of LFP remains lower than that of LMFP due to its relatively low average electrode potential (~3.4 V *vs.* Li^+/Li)[6]. In contrast, LMFP, which is isostructural to LFP, offers at least 10% higher electrode potential (> 3.8 V) and energy density (> 646 W h kg^{-1})[7]. Other advantages of LMFP include a cost-effective synthesis process similar to that of LFP and high compatibility with NCM within the operating voltage range of commercial LIBs[8]. Battery manufacturers worldwide are independently driving the development of high-performance LIBs utilizing LMFP as a cathode, either alone or in combination with NCM. Therefore, understanding the fundamental physicochemical properties of LMFP and the cell parameters is essential for designing LMFP-based LIBs.

The average discharge potential of LMFP, a solid solution of LFP and $LiMnPO_4$ (LMP), is determined by the Mn/Fe mixing ratio and lies between the low Fe^{3+}/Fe^{2+} redox potential of LFP and the high Mn^{3+}/Mn^{2+} redox potential of LMP[5,9]. As the Mn content (1-y) in LMFP increases, additional Mn^{3+}/Mn^{2+} redox reactions are activated at a potential plateau of around 4.1 V, enhancing the operating voltage and energy density of LMFP cells[10,11]. In addition, the side reactions of LMFP with typical organic electrolytes are relatively suppressed compared with those of high-voltage cathode oxides because of the lower reactivity between the phosphates on the LMFP particle surface and the neighboring electrolyte species[12,13]. In contrast, the detrimental Mn dissolution and Jahn-Teller distortion induced by the Mn^{3+} ions generated during Li-ion extraction from LMFP became more pronounced, particularly at elevated temperatures[14], as illustrated schematically in Figure 1. Additionally, the facile formation and movement of Mn^{3+}/Mn^{2+} phase boundaries within LMFP particles hinder Li-ion diffusion during cycling[15]. These conflicting effects suggest that increasing the Mn content in LMFP enhances the theoretical energy density, while compromising its thermal stability. Therefore, elucidating the charge/discharge reaction mechanism in conjunction with the phase transition of LMFP is critical. However, these properties are highly dependent on factors such as the Mn/Fe mixing ratios[16,17], synthesis methods[18-21], applied current densities[22], and particle size/crystallinity/orientation[23-26].

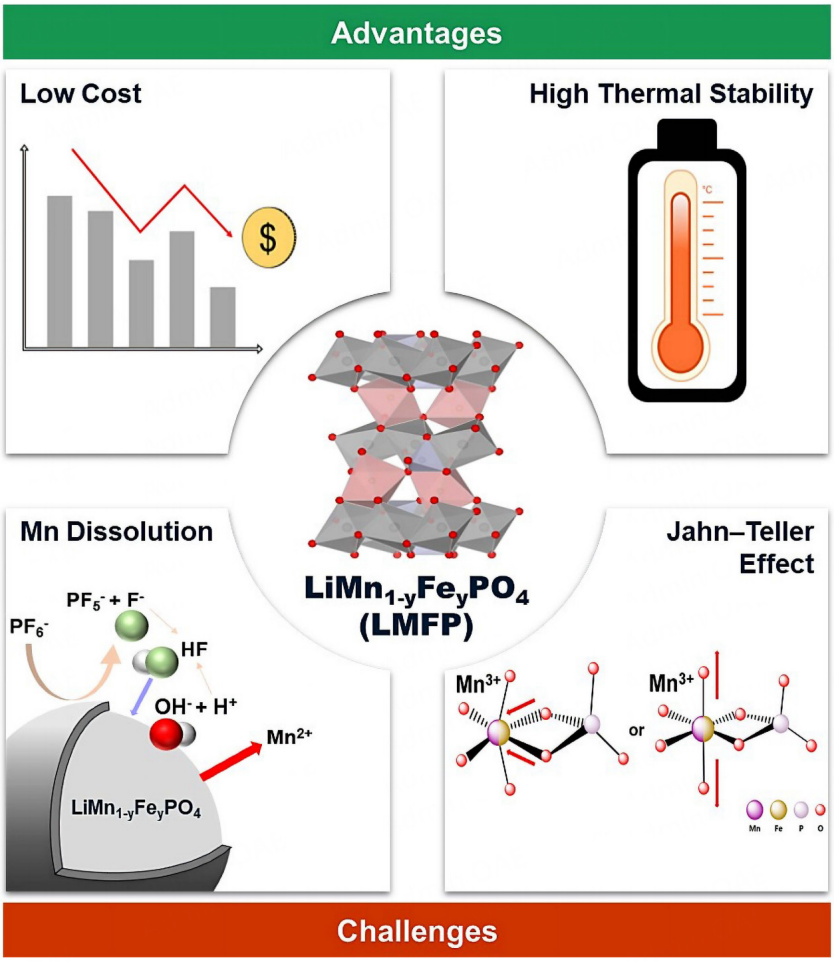

Figure 1. Advantages and challenges of $LiMn_{1-y}Fe_yPO_4$ (LMFP) cathode materials for Li-ion rechargeable batteries (LIBs).

Although interpreting these complexities remains challenging, high-quality reviews have comprehensively addressed the underlying relationship between the physical and electrochemical performances of LMFP cathodes in half-cell configurations using lithium metal anodes[3,14,16,27-29]. This concise review primarily focuses on recent research trends and progress in LMFP-based full-cell systems, including LMFP/graphite and LMFP/$Li_4Ti_5O_{12}$ (LTO), with comparisons to commercial LFP-based counterparts. Finally, we highlight the challenges and prospects of LMFP materials and cell designs for the development of LIB technology.

$LiMn_{1-y}Fe_yPO_4$ RECHARGEABLE BATTERIES

Critical considerations in advanced LMFP battery design

The key aspects of $LiMn_{1-y}Fe_yPO_4$ (LMFP) full-cell design include optimizing the LMFP cathode and compatible anode materials, enhancing the electronic/ionic conductivities of the electrodes, minimizing interfacial resistances between different phases, and improving the structural and thermal stability of cell components. Battery manufacturers can assess the viability of the LMFP cathode through electrochemical testing with LMFP full cells. Thus, optimizing full-cell design is essential for achieving maximum performance. The first step in LMFP full-cell design is defining the target cell capacity and voltage based on the application-specific requirements, including minimum cell capacity, nominal operating voltage, and safety considerations. These cell requirements are closely linked to various physical parameters of the cell

components, such as the number of stacked electrodes (cathodes and anodes), the area ratio of the active electrodes to inactive regions, active material (LMFP and anode materials) loading, the mass ratio of active material to conductive agent, and binder, the negative-to-positive (N/P) ratio (i.e., the ratio of anode capacity to cathode capacity), the reduction ratio of electrode thickness (the ratio of initial thickness to final thickness), electrode density, the thickness of the current collector and separator, the weight and thickness of the cell packaging, and electrolyte volume [Figure 2]. From a commercialization standpoint, a stepwise design of LMFP cells, electrodes, and materials is the most effective approach.

Among these cell parameters, the N/P ratio is one of the most critical, as achieving a proper balance between the cathode and anode is essential for maximizing energy density, enabling fast charging, and maintaining a high level of safety in LMFP full cells. To accurately adjust the N/P ratio based on cell design requirements, preliminary LMFP and anode half-cell tests are conducted to verify initial and reversible capacities[2]. In general, the N/P ratio in conventional LIBs ranges from 1.05 to 1.15 to ensure high capacity and superior cycle life, with the anode capacity slightly exceeding that of the cathode. This ratio can be fine-tuned by controlling the active material loading on both electrodes, and a similar approach can be applied to LMFP full cells.

An N/P ratio below unity can enhance initial performance by maximizing anode material utilization and reducing the reaction potential. However, it often introduces significant safety concerns, such as Li plating and dendrite formation on the anode surface due to localized current concentrations during cycling, ultimately leading to rapid capacity degradation and safety risks. Conversely, a higher N/P ratio mitigates Li plating and improves cycling stability by providing additional Li storage capacity and reducing stress on the anode. However, this approach also reduces energy density and increases material costs, making it less desirable for high-performance applications. Consequently, optimizing the N/P ratio to balance high energy density, safety, and cost remains a key focus in the research and development of LMFP batteries.

In the battery industry, maximizing energy density within limited cell space requires not only optimizing the N/P ratio from an electrode perspective but also improving other parameters, such as electrode density and the area ratio between the anode and cathode. The first approach involves maximizing the reduction ratio of electrode thickness to bring the electrode density as close as possible to its theoretical value. The LMFP cathode material, which has a bimodal particle size distribution consisting of small and large particles, was appropriately mixed and applied to the LMFP cathode. However, as the electrode density of the LMFP cathode increases, the penetration of the electrolyte into the electrode during discharge and charge cycles, as well as Li-ion diffusion, becomes more difficult, leading to rapid degradation of cell performance. Therefore, the development of a novel high-density LMFP cathode design capable of overcoming these limitations is critical. The second approach focuses on minimizing the difference in the area ratio between the anode and LMFP cathode. Typically, the cathode area is at least 20% smaller than that of the anode. However, to achieve high energy density in LMFP full cells, industrial designs aim to minimize the difference, ensuring that the cathode remains only slightly smaller than the anode. If the area difference becomes too small, excessive Li deposition on the edges of the anode may occur, promoting Li dendrite growth and increasing the risk of cell failure. Thus, careful attention is required when designing electrode areas.

In addition, LMFP cathode materials pose a potential risk related to overcharging due to the distinct potential plateau around 4.1 V, corresponding to the Mn^{3+}/Mn^{2+} redox reactions. Since the high operating potential remains constant during charging, it is difficult to determine the exact end point of the process. This issue is critical when designing safer LMFP full cells. Therefore, combining the LMFP cathode with a

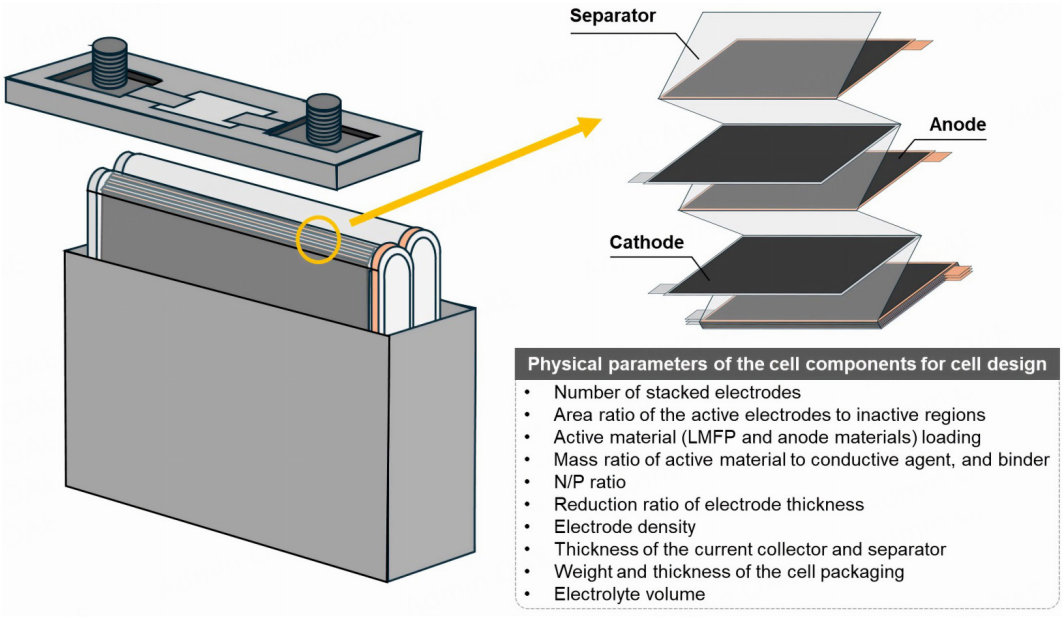

Figure 2. Key parameters for the practical design of LMFP full cells.

compatible anode is crucial, as the charge/discharge profiles, operating voltage, capacity, power, and safety of LMFP full cells are significantly influenced by the electrochemical and physicochemical properties of the anode materials[30]. A detailed discussion on this topic is presented in the following section.

Recent advances in LMFP/graphite battery technology

Graphite anodes play a pivotal role in conventional LIBs, where initial Li loss occurs during the formation of the solid electrolyte interphase (SEI) layer on the surfaces of graphite particles. The SEI layer forms through the reduction of the electrolyte on the graphite surface during the initial discharging process, which contributes to maintaining the stability of the anode. Specifically, it prevents subsequent Li loss induced by continuous electrolyte decomposition on the anode surface throughout cycling, thereby significantly improving the long-term cycling performance of the graphite anode.

While LMFP cathodes exhibit remarkable rate capabilities, the dissolution of transition metals, particularly Mn and Fe, poses a significant challenge, leading to severe capacity fading in both LMFP half and full cells. Dissolved metal cations in the electrolyte migrate to the anode, where they are reduced, resulting in the degradation of the SEI layer on the graphite electrodes[31]. X-ray photoelectron spectroscopy (XPS) analysis of $LiMn_{0.67}Fe_{0.33}PO_4$ electrodes, compared to LFP electrodes, demonstrated a significant reduction in CO_3 and CO phases upon discharge, indicating SEI layer decomposition on graphite anodes[32].

The higher operating potential of the LMFP electrodes exacerbates reactivity, leading to Mn reduction and further degradation of the SEI layer. This layer, essential for the electrochemical protection of the anode surface, prevents continuous electrolyte decomposition during cycling and minimizes initial Li loss. Graphite anodes benefit from stable SEI phases, providing higher coulombic efficiency compared to alloy-based anodes, where the SEI layers are unstable and exhibit continuous growth. However, reduced transition metals accelerate SEI formation, contributing to irreversible capacity loss. Mn-induced parasitic reactions in the SEI also cause gas evolution due to electrolyte decomposition. Neutron imaging and Prompt Gamma Activation Analysis (PGAA) have shown that LMFP/graphite cells generate approximately

30% more gas than LFP/graphite cells, attributed to Mn deposition on the anode[33]. While LMFP/graphite cells exhibit a higher initial capacity loss than LFP/graphite cells, they demonstrate superior long-term cycling performance as Mn dissolution decreases with cycling.

To mitigate transition metal dissolution, particularly that of divalent Mn, many studies have focused on stabilizing the surface of LMFP cathode materials. Surface coatings with robust outer layers have proven effective in enhancing cell performance. Elevated temperatures (e.g., 60 °C) and higher operating voltages accelerate the decomposition of the electrolyte salt ($LiPF_6$), leading to hydrofluoric acid (HF) formation and decomposition of oxide-based active materials. Applying an LFP outer layer, resistant to HF, on $LiMn_{0.85}Fe_{0.15}PO_4$ cathode materials has shown significant improvements[34]. A 0.5 μm LFP coating on LMFP reduced Mn and Fe dissolution by over 50% compared to uncoated LMFP. Full-cell tests with graphite anodes demonstrated capacity retention of over 97% for LMFP/LFP electrodes, whereas uncoated LMFP electrodes exhibited lower stability after cycling at 60 °C and a current density of 0.5 C within the voltage range of 2.7-4.5 V. Furthermore, LMFP/LFP electrodes exhibited superior rate capabilities, delivering ~90 mA h g^{-1} at 5 C compared to ~75 mA h g^{-1} for uncoated LMFP electrodes.

Several studies have investigated the surface modification of LMFP cathode materials using other strategies such as electrolyte modification and doping. Theivanayagam *et al*. have explored water-based protective coatings, such as SiF_4 on $LiMn_{0.8}Fe_{0.2}PO_4$, to enhance surface stability[35]. In the absence of surface treatments, simple mixing of electrolyte additives offers a cost-effective industrial approach. For instance, using lithium difluoro(oxalate)borate (LiDFOB) or lithium bis(trifluoromethanesulfonyl)imide (LiFSI) salts in adiponitrile (ADN)/dimethyl carbonate (DMC) electrolytes enables graphite anode operation without fluoroethylene carbonate (FEC) additives, which are required for anodic stability[36]. ADN-based electrolytes with LiDFOB facilitated stable cycling of $LiMn_{0.63}Fe_{0.37}PO_4$/graphite full cells [Figure 3A]. The SEI formed in ADN/DMC electrolytes with LiFSI and LiDFOB exhibited higher thermal stability than those formed in conventional ethylene carbonate (EC)-based electrolytes, with exothermic reaction onset temperatures of 150-160 °C, compared to 110 °C for EC/DMC electrolytes [Figure 3B].

In addition, considerable attention has been devoted to understanding the relationship between Mn dissolution and different crystal surfaces of LMFP as Mn dissociation strongly depends on the local lattice distortions associated with the Jahn-Teller effect. Lv *et al*. investigated the effects of Mg, V and Co doping in $LiMn_{0.5}Fe_{0.5}PO_4$ cathode materials using first-principle calculations[37]. Among these, Mg doping yielded the lowest formation energy and the lowest volume change rate, leading to the mitigation of the Jahn-Teller effect[37]. Li *et al*. reported the effect of surface concentration of Fe and Mn on the electrochemical performance of LMFP, based on the electronic differences between Mn^{3+} and Fe^{3+} in MO_6 octahedra[38]. From density functional theory (DFT) calculations, volume changes and binding energies with HF during charging were analyzed. Based on these results, an LMFP/C cathode material with a Fe-rich and a Mn-deficient surface layer (~2 nm) was synthesized, which exhibited enhanced electrochemical performance. This improvement was attributed to the suppression of Mn dissolution and stabilization of crystal lattice compared to undoped LMFP/C[38].

Although LMFP electrodes are cost-effective, safe, and exhibit stable cycling performance, they do not satisfy the energy density requirements for long-range electric vehicles (EVs). Among available cathode materials, NCM cathode materials offer the highest energy density, meeting automotive industry demands. Blending $LiMn_{0.6}Fe_{0.4}PO_4$ with NCM improves the energy density of the cells, while reducing charge-transfer resistance by enhancing Li-ion diffusion coefficients. LMFP displays voltage plateaus at 3.9-4.2 and 3.4-3.6 V, with a rapid voltage drop after discharging to 3.0 V. The voltage range of NCM is similar to that

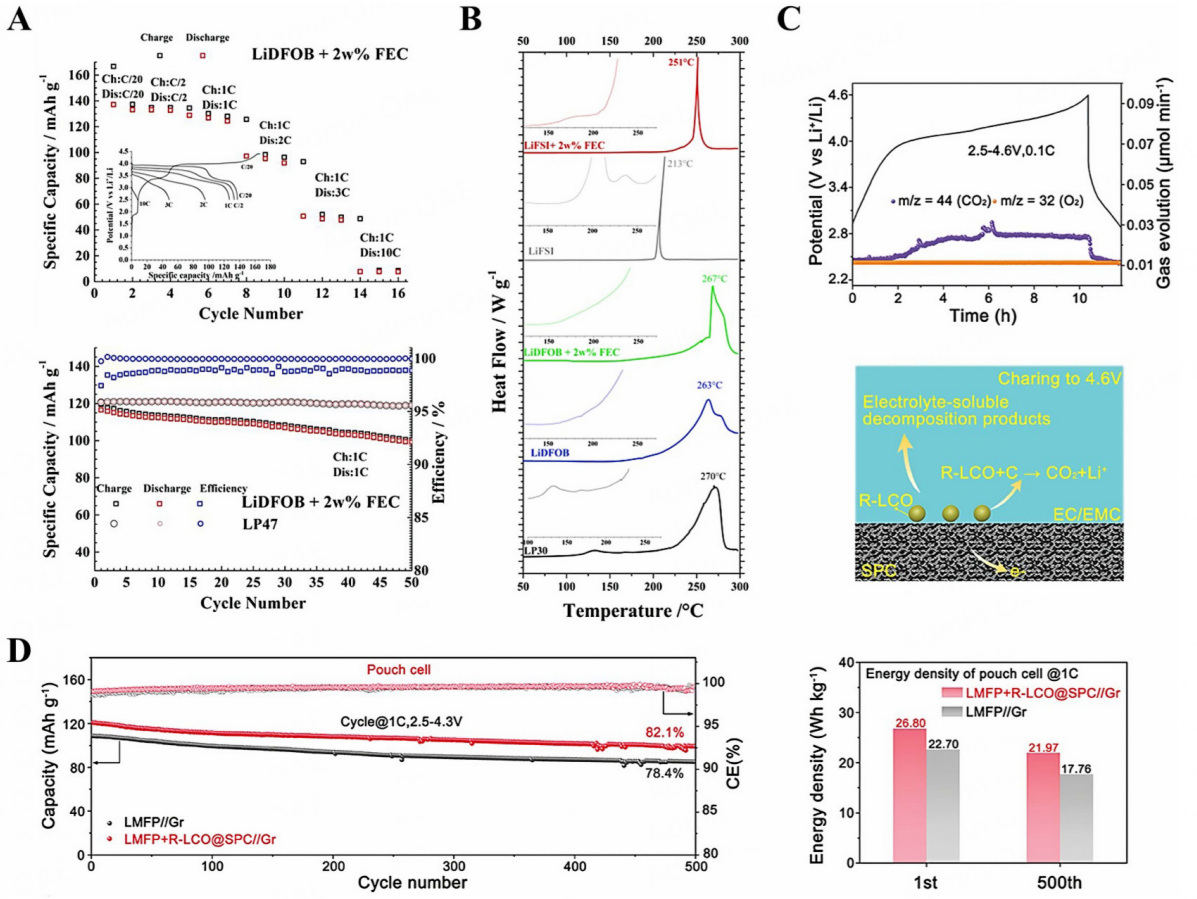

Figure 3. (A) Rate capability and cycling stability of LMFP/graphite full cells tested in ADN/DMC (1:1, weight ratio) electrolyte with 2 wt% FEC in 1 M LiDFOB. (B) DSC analysis results for 1 M ADN/DMC (1:1, weight ratio) electrolytes. Reproduced with permission from[36]. Copyright © 2018 Elsevier. (C) In situ DEMS analysis results and (D) decomposition pathways of Li_2CO_3 as a Li compensation agent. Reproduced with permission from[42]. Copyright © 2024 John Wiley & Sons, Inc.

of LMFP under 3.0-4.2 V, enabling synergistic effects in blended materials. Electrochemical analysis of blended electrodes revealed three distinct redox peaks at 3.9-4.2, 3.6-3.9, and 3.4-3.6 V, corresponding to Mn^{3+}/Mn^{2+}, Ni^{4+}/Ni^{2+}, and Fe^{3+}/Fe^{2+} redox reactions, respectively. These blended electrodes demonstrated improved electrochemical kinetics, including lower charge-transfer resistance and higher Li-ion diffusion coefficients, leading to superior rate capability, low-temperature performance, and high-temperature stability[39-41]. Table 1 summarizes the components and key electrochemical performances of representative LMFP-NCM/graphite 18650 full cells.

Pre-lithiation is a promising strategy to compensate for irreversible Li consumption during SEI formation and side reactions in full cells. The initial Li loss primarily occurs due to SEI formation on the anode surfaces. While pre-lithiation agents, such as Li silicides, Li alloys, and stabilized Li powders, can address this issue, their high reactivity with oxygen and moisture poses safety challenges, particularly during anode material preparation in aqueous environments. Alternative methods include direct Li deposition on anode surfaces; however, this approach carries risks such as uneven lithiation, excessive lithiation, structural damage, dendritic growth, and N/P ratio imbalances.

Table 1. Components and electrochemical performances of representative LMFP-NCM/graphite 18650 full cells

LMFP composition	NCM composition	Blending ratio	Window voltage (V)	18650 cell capacity (mA h@C-rate)	Capacity retention (%@cycles)	Ref.
$LiMn_{0.6}Fe_{0.4}PO_4$	NCM523	30:70	3.0-4.2	2,024@1C	96.2@500	[37]
$LiMn_{0.6}Fe_{0.4}PO_4$	NCM523	70:30	2.5-4.2	1,954@0.5C	97.7@250	[38]
$LiMn_{0.6}Fe_{0.4}PO_4$	NCM523	-	2.5-4.2	2,000@1C	82.6@1,000	[39]

NCM523: $LiNi_{0.5}Co_{0.2}Mn_{0.3}O_2$

In contrast, cathode pre-lithiation involves introducing a stable Li compensation agent, such as Li_2CO_3, to the cathode slurry. During initial charging, Li_2CO_3 releases Li ions, compensating for SEI-related Li consumption and improving cycle stability[42]. However, the high decomposition potential of Li_2CO_3 lowers initial coulombic efficiency. To address this issue, carbon materials rich in carbonyl (C=O) groups can act as catalytic sites for Li_2CO_3 decomposition at lower potentials [Figure 3C]. In LMFP/graphite full cells, using carbon substrates with C=O groups resulted in ~82.1% capacity retention after 500 cycles at 1 C, representing a 19.1% increase in energy density compared to cells without pre-lithiation [Figure 3D].

Recent advances in LMFP/$Li_4Ti_5O_{12}$ (LTO) battery technology

A recent study demonstrated the synergistic effects of Nb and Mg co-doping on the surface kinetics and bulk stability of carbon-coated $LiMn_{0.5}Fe_{0.5}PO_4$ particles. The introduction of Nb facilitated the formation of $LiNbO_3$ surface coating layers, enhancing Li ionic conductivity, while a small amount of Mg effectively replaced divalent transition metal (Fe^{2+}/Mn^{2+}) sites, mitigating the structural distortion in LMFP caused by the Jahn-Teller effect of Mn^{3+} ions. Consequently, an LMFP/graphite full cell with 1 mol% Nb and 3 mol% Mg in the LMFP cathode exhibited outstanding cycling performance, retaining 99% of its capacity over 300 cycles at a current density of C/2. Nevertheless, the capacity degradation during cycling was more pronounced in the LMFP/graphite full cell than in the LMFP/Li half cell, primarily attributed to the loss of Li inventory associated with unstable SEI layers forming on the graphite anode surface[43].

The first LMFP/LTO full cells were systematically evaluated for their potential applications in load leveling to support the widespread adoption of renewable energy, which requires exceptional power and safety characteristics[44]. Despite the inherently higher Ti^{4+}/Ti^{3+} redox potential (~1.5 V *vs.* Li^+/Li) and lower theoretical capacity (~175 mA h g^{-1}, LTO + 3Li + $3e^-$ ↔ $Li_7Ti_5O_{12}$), which limit the energy density of the battery cells, LTO has garnered significant attention as a promising alternative to graphite anodes[45]. The primary advantage of LTO lies in its robust "zero-strain" spinel structure, which minimizes lattice changes during cell operation, ensuring exceptional thermal stability (safety) and structural integrity (cycle life) in LTO-based full cells. Additionally, the facile Li-ion diffusion through the three-dimensional pathways within the spinel structure enhances the power density of the cell. Furthermore, unlike graphite, LTO suppresses the formation of undesirable SEI layers and the growth of Li dendrites due to its higher voltage window, as shown in Figure 4A, which exceeds the thresholds for reductive electrolyte decomposition and Li electroplating. This characteristic also enables the use of thinner and more cost-effective Al foil as a current collector in LTO anodes instead of Cu foil. Notably, the viability of $LiMn_{0.8}Fe_{0.2}PO_4$/LTO full cells as stable energy storage devices was assessed in this study, demonstrating a high reversible capacity of ~150 mA h g^{-1} at a low current density of C/10. However, further optimization of the cells is required.

A subsequent investigation systematically analyzed the electrochemical behaviors of $LiMn_{0.8}Fe_{0.2}PO_4$/LTO full cells cycled at 30 and 60 °C[46]. While the initial discharge capacity of the LMFP/LTO cells remained constant at 30 °C, the cells experienced severe capacity fading within 100 cycles, induced by the loss of active Li from the electrodes rather than the dissolution of divalent transition metal ions (particularly Mn^{2+}) from

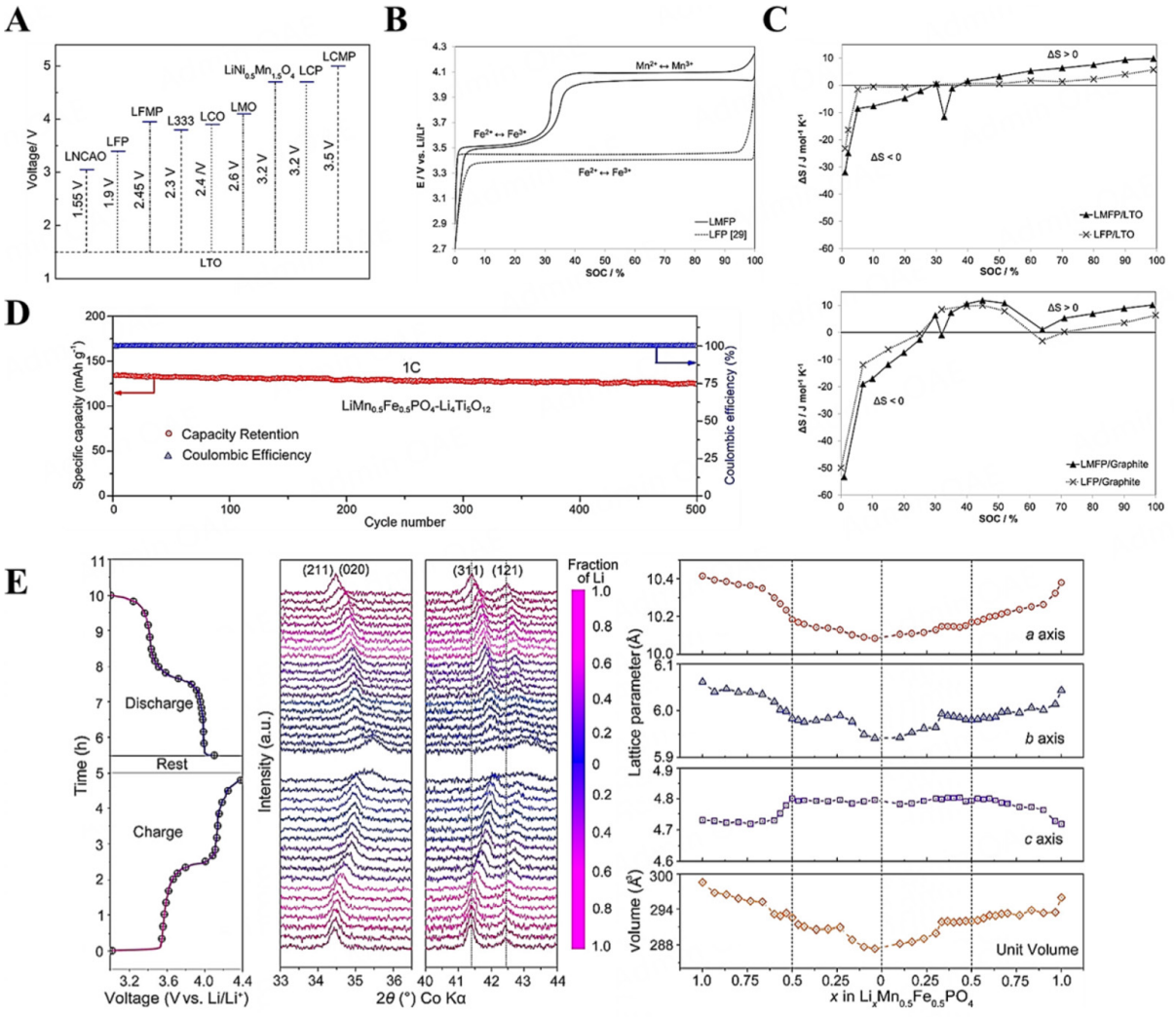

Figure 4. (A) Operating voltage of an LTO anode and typical cathode materials. Reproduced with permission from[45]. Copyright © 2017 Elsevier. (B) Charge/discharge profiles of LMFP and LFP half cells as a function of SOC. (C) Calculated entropy change of LMFP/LTO, LFP/LTO, LMFP/graphite, and LFP/graphite full cells. Reproduced with permission from[47]. Copyright © 2015 Elsevier. (D) Long-term cycling stability of $LiMn_{0.5}Fe_{0.5}PO_4$/LTO full cell at a current density of 1 C. (E) In situ structural characterization of $LiMn_{0.5}Fe_{0.5}PO_4$ during the charge/discharge process. Reproduced with permission from[48]. Copyright © 2021 American Chemical Society.

LMFP into the electrolyte. To further assess electrode stability, LMFP cathodes and LTO anodes were collected from disassembled LMFP/LTO cells after prolonged cycling at 60 °C, and reused in separate LMFP/Li and LTO/Li half cells. These electrodes exhibited excellent cycling performance at 30 °C, comparable to that of half cells assembled with pristine LMFP and LTO electrodes. More importantly, the electrochemical stability of LMFP/LTO full cells operated at elevated temperatures was improved by combining a pre-passivated LTO anode, activated during cycling in LMFP/LTO full cells at 60 °C with a pristine LMFP cathode. This indicates that the surface reactions between the LTO anodes and electrolytes, such as the reduction of alkyl carbonates or $LiPF_6$ salts, become more pronounced at higher temperatures, leading to the loss of active Li. However, the LTO anode itself undergoes minimal degradation. As a result, the pre-passivated LTO significantly mitigates thermal deterioration in LMFP/LTO full cells, even at temperatures up to 60 °C.

To assess potential risks in large-scale LIBs under harsh environmental conditions, the thermal stability of LMFP/LTO full cells was examined by analyzing the entropy change (ΔS) of both the cathode and anode as a function of the state of charge (SOC)[47]. ΔS was estimated from the derivative of the open-circuit voltage (OCV) with respect to temperature, which correlates with the amount of heat generated by the electrodes during cell operation. A sharp change in ΔS was observed in $LiMn_{0.67}Fe_{0.33}PO_4$ within the intermediate Fe-Mn transition region, where a single-phase solid-solution reaction occurred, as exemplified by $Li_{0.33}Mn_{0.67}Fe_{0.33}PO_4$. Similarly, the graphite anode showed significant variations in ΔS due to its complex staging behavior during Li-ion intercalation and deintercalation. In contrast, the LFP cathode and LTO anode, both characterized by a two-phase reaction mechanism across nearly the entire SOC range [Figure 4B], exhibited an almost constant ΔS within the same SOC region. According to $\Delta S_{\text{full cell, discharge}} = \Delta S_{\text{cathode, reduction}} + \Delta S_{\text{anode, oxidation}}$, the ΔS of LFP/LTO full cells was close to zero due to the offset between the individual ΔS_{LFP} and ΔS_{LTO}, which have similar absolute values but opposite signs. However, the ΔS of LMFP/LTO full cells deviated further from zero compared to LFP/LTO full cells [Figure 4C], indicating a higher rate of heat generation and release across the entire SOC range. Unlike other graphite-based full cells, including LMFP/graphite and LFP/graphite, LMFP/LTO full cells exhibited the potential for reversible heat generation and consumption.

Reducing the particle size of LMFP to the nanoscale facilitated a one-phase transition throughout the entire cycling process, with the Li miscibility gap progressively narrowing as the particle size decreased. For instance, $LiMn_{0.5}Fe_{0.5}PO_4$ nanocrystals (< 150 nm) with equimolar Mn and Fe showed an impressive discharge capacity of ~104 mA h g^{-1} at a high current density of 10 C. This improvement was attributed to the presence of short Li-ion diffusion paths and the absence of the sluggish two-phase Mn^{3+}/Mn^{2+} transition in LMFP nanocrystals during cycling[48]. Additionally, the cycling-dependent volume change in the olivine lattice was smaller for LMFP with a zero miscibility gap than for LFP, which typically undergoes Fe^{3+}/Fe^{2+} two-phase reactions, thereby contributing to the extended lifespan of LIBs. A full cell assembled with the LMFP cathode and LTO anode delivered a specific capacity of ~124 mA h g^{-1} at a current density of 1 C after 500 cycles, corresponding to ~92.5% of its initial cell capacity [Figure 4D]. The superior power and cycling performance of the LMFP/LTO full cell can be attributed to the excellent rate capabilities of both electrodes, including the facile Li-ion diffusion during the extended one-phase transition of nanoscale LMFP [Figure 4E].

To address the intrinsically low electrical conductivity and surface instability of LMFP cathode materials, two highly effective strategies were employed: compositing LMFP particles with conductive materials and applying carbon coatings to their surfaces [Figure 5A]. These approaches significantly enhanced the electrical conductivity and electrochemical stability of the LMFP surfaces, contributing to the high power output and extended cycle life of LMFP/LTO full cells. The reported combinations of carbon sources that improve electrical conductivity and complexing agents that regulate the atmosphere include carbon black/sucrose and polystyrene/citric acid[49,50]. Notably, electrically conductive carbon nanotube (CNT)-embedded $LiMn_{0.8}Fe_{0.2}PO_4$/C microspheres demonstrated an outstanding discharge capacity of ~121 mA h g^{-1}, even at a high current density of 20 C[51], as exhibited in Figure 5B. Additionally, CNTs offer exceptional mechanical strength, effectively preserving the electrical network and accommodating volume changes in LMFP/C microspheres during electrochemical cycling. Consequently, a full cell employing CNT-embedded LMFP/C as the cathode paired with a high-power LTO anode achieved a discharge capacity exceeding 130 mAh g^{-1} at a high current density of 10 C.

Meanwhile, Li_3VO_4/carbon hybrid conductors were introduced as ionic/electronic dual-conductive layers on the surfaces of $LiMn_{0.5}Fe_{0.5}PO_4$ nanorods (100-200 nm)[52]. These conductive materials also function as

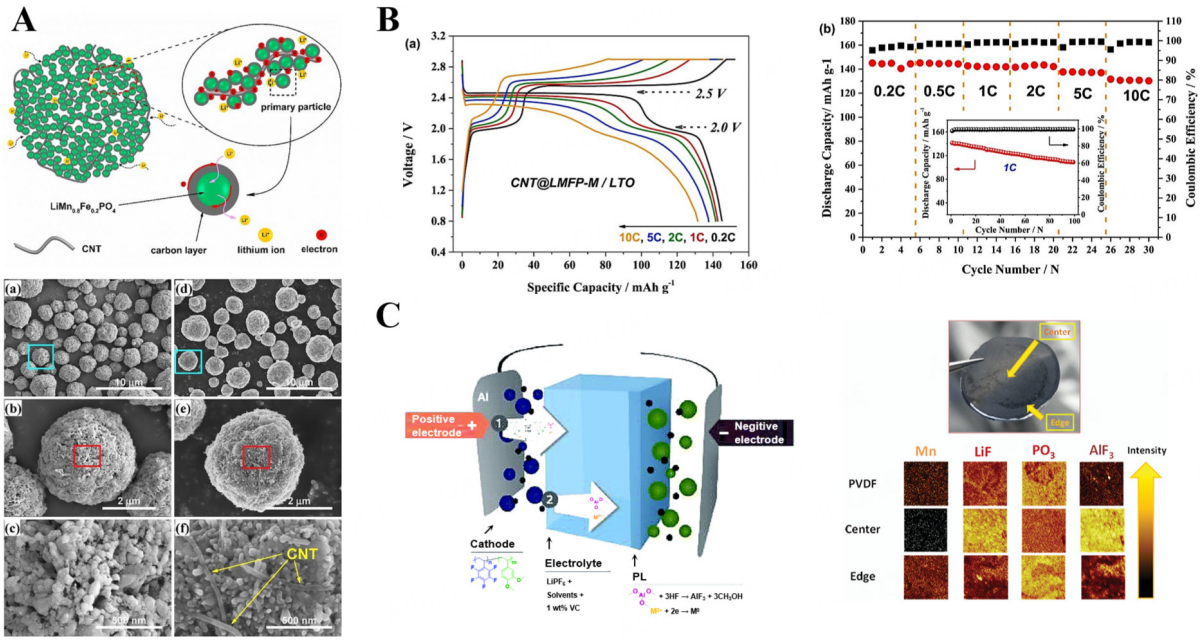

Figure 5. (A) Morphology of micro-spherical $LiMn_{0.8}Fe_{0.2}PO_4$ and CNT composites. (B) Charge/discharge profiles and rate capability of CNT@LMFP/LTO full cells. Reproduced with permission from[51]. Copyright © 2018 Elsevier. (C) Proposed mechanism of protecting layer (PL) formation on the surface of LTO anode induced by the incorporation of 2,3-dimethoxystyrene into the PVDF binder. Reproduced with permission from[53]. Copyright © 2021 Royal Society of Chemistry.

surface protectors, mitigating detrimental interfacial reactions between the LMFP nanorods and the electrolyte. The optimal conditions for the composition design and synthesis of this complex enabled the realization of its excellent rate capability (~125 mA h g^{-1} at 10 C) and cycling retention properties (~120 mA h g^{-1} at 5 C after 1,000 cycles, corresponding to a low capacity loss of 0.0085% per cycle), comparable to those of CNT-embedded LMFP/C microspheres. However, in this study, the capacity retention of the LMFP nanorod/LTO full cells after 120 cycles at a current density of 1 C was ~74.3%, which was substantially lower than the value observed in the cycling behavior of the hybrid-coated LMFP half cells. Further investigation is required to understand the disparity in the electrochemical performance between LMFP half and full cells.

In LMFP/LTO full cells, Mn^{2+} ions released from the LMFP cathode surface diffuse through the electrolyte toward the opposing LTO anode, where they ultimately deposit on its surface. The deposited Mn^{2+} ions are then reduced to Mn metal, which catalyzes undesirable electrolyte decomposition side reactions. One of the most effective approaches for mitigating the interaction between Mn^{2+} ions and the electrolyte involves incorporating a functional polymer (e.g., 2,3-dimethoxystyrene) into the polyvinylidene fluoride (PVDF) binder, which coordinates with multivalent metal ions in LMFP, thereby suppressing their dissolution and diffusion[53]. The incorporation of this polymer additive enhanced the capacity retention of $LiMn_{0.75}Fe_{0.20}Mg_{0.05}PO_4$/LTO full cells by 16.7% over 300 cycles at 1 C and 45 °C. This improvement can be attributed to two primary factors: (1) the suppression of Mn^{2+} ion dissolution into the electrolyte, which maintained the reversibility of Mn^{3+}/Mn^{2+} redox reactions in LMFP; and (2) the formation of a protective layer on the LTO anode, preventing surface degradation and electrolyte decomposition [Figure 5C].

Feasibility of alternative LMFP-based battery technologies

In addition to LMFP/graphite and LMFP/LTO full cells, LMFP-based full cells incorporating ceramic metal oxide and metallic alloy anodes have demonstrated superior cell capacity and energy density compared to

conventional configurations. Yang *et al.* combined 1 wt% LTO-coated $LiMn_{0.5}Fe_{0.5}PO_4$/C as the cathode and a graphite/SiO_2/C composite as the anode for LIBs[54]. As a coating material on LMFP particles rather than as an anode material, LTO remained electrochemically inactive within the high-voltage range of LMFP half and full cells. However, even at 60 °C, a trace amount of LTO (1 wt%) effectively suppressed the dissolution of Mn^{2+} and Fe^{2+} ions from the LMFP surfaces into the electrolyte. Additionally, the intrinsically conductive nature of the LTO layers on the surfaces of the LMFP particles facilitated Li-ion solvation and desolvation while providing physical protection against HF attacks. Consequently, the full cell assembled with the LTO-coated LMFP/C cathode and high-capacity graphite/SiO_2/C anode demonstrated excellent power and long-term cycling stability.

Metal oxides such as Fe_2O_3 and Fe_3O_4 undergo electrochemical charge and discharge processes based on conversion reactions, achieving high theoretical capacities of ~1,007 mA h g^{-1} for Fe_2O_3 and ~926 mA h g^{-1} for Fe_3O_4[55,56]. The initial coulombic efficiency and reaction reversibility of these materials can be enhanced by nanosizing the active particles and drying the active electrodes above the melting point of the PVDF binder. In particular, preheating the pristine electrodes at 250 °C prior to cycling enhances adhesion between Fe_2O_3 or Fe_3O_4 nanoparticles, binders, and the current collector, thereby mitigating cycling-induced volume changes of the metal oxides and preventing disconnection among the electrode components. This approach preserved the initial discharge capacity (> 1,000 mA h g^{-1}) of Fe_3O_4 for up to 1,000 cycles in Fe_3O_4 half cells. However, $LiMn_{0.8}Fe_{0.2}PO_4/Fe_3O_4$ full cells, despite achieving a cell voltage of ~2.0 V and a cell capacity of ~130 mA h g^{-1} based on cathode loading, exhibited degradation within 10 cycles, accompanied by significant voltage hysteresis due to the conversion reaction of the Fe_3O_4 anode. High-performance Sn/C or Sn/Fe_2O_3/C composites have also been employed as anode materials for LMFP full cells[57,58]. To avoid the severe degradation of metallic anodes caused by large volume changes, the utilization of these active materials was restricted during full-cell operation by increasing the N/P ratio. Consequently, the capacity fading of the LMFP cathode was minimized relative to that of the Sn/C or Sn/Fe_2O_3/C anodes. However, the utilization of anode materials remains crucial for maximizing cell capacity and energy density.

Key opportunities and challenges in LMFP battery technology

Enhancing the electrochemical and thermal properties of LMFP full cells requires a comprehensive technological approach, including the optimization of LMFP cathodes, integration of compatible anodes and electrolytes, and establishment of stable cell operating conditions. These aspects are addressed individually in the subsequent subsections.

Advancing LMFP cathodes for practical applications

LMFP faces challenges related to its low electronic conductivity and sluggish Li-ion diffusion kinetics, which result in inferior rate capability[6]. Additionally, the pronounced Jahn-Teller distortion and Mn dissolution into the electrolyte, driven by an increase in Mn^{3+} ions in LMFP during charging, lead to unstable cycling performance at elevated temperatures compared to commercial LFP[59,60]. To overcome these issues, surface protection of LMFP particles with conductive carbon is considered crucial, with an emphasis on optimizing the uniformity, content, and degree of graphitization of the coated carbon[61-63]. A promising approach involves the construction of three-dimensional conductive networks using highly graphitized graphene or CNTs on the surfaces of LMFP particles. In addition to carbon coating, reducing the particle size of LMFP to the nanoscale is an effective strategy for enhancing power performance by shortening the Li-ion diffusion path within the bulk[18,64]. However, while carbon coating decreases the tap density of the LMFP, nanosizing increases the reactive surface area in contact with the electrolyte, negatively affecting the volumetric energy density and cycling performance. Therefore, the ideal morphology of the LMFP particles consists of porous microscale secondary particles sparsely aggregated with LMFP nanoparticles, with a minimal yet uniformly distributed conductive carbon coating on the primary

nanoparticles[65].

The theoretical specific energy density of LMFP increases with increasing Mn content (1-y). However, when 1-y exceeds 0.8, the practical electrochemical performance of LMFP deteriorates due to compositional and physicochemical similarities with LMP. Thus, the Mn content in the range of 0.5 to 0.8 is generally considered suitable for LMFP applications, depending on whether a fast discharge rate or extended cycle life is required. Despite extensive efforts, the exact relationship among Mn/Fe ratios, SOC-dependent phase transitions, and electrochemical cycling performance of LMFP remains intricate and not yet fully understood[16]. Nevertheless, several consensus approaches have been established based on precise electrochemical and in situ structural analyses. Compared to Mn^{3+}/Mn^{2+}, Fe^{3+}/Fe^{2+} redox reactions are more likely to exhibit a single-phase solid solution transition, particularly in the intermediate stages of charge and discharge, regardless of the Mn/Fe ratio in the LMFP[66]. In general, Mn^{3+}/Mn^{2+} redox reactions follow a two-phase transition mechanism, even when Fe content exceeds that of Mn (i.e., $1\text{-}y < 0.5$). Additionally, as the Mn/Fe ratio increases, the two-phase transition region corresponding to the Mn^{3+}/Mn^{2+} redox reactions steadily expands[17].

Due to these differences in transition mechanisms, the Li-ion diffusivity in the Mn^{3+}/Mn^{2+} reaction region is consistently lower than in the Fe^{3+}/Fe^{2+} reaction region[28,67]. The inherent limitations imposed by nucleation and growth kinetics during cycling further hinder the kinetics of two-phase transition reactions. This effect is exacerbated by the Jahn-Teller effect, which distorts the Mn-O bonds in the LMFP lattice and induces a lattice mismatch, reducing the number of Li-ion diffusion channels and increasing the activation energy barrier for Li-ion migration. Additionally, the inhomogeneous distribution of Mn and Fe weakens their mutual interactions, thereby influencing the electronic structure of LMFP during cycling. Specifically, the significantly slower kinetics of the Mn^{3+}/Mn^{2+} redox reactions compared to that of the Fe^{3+}/Fe^{2+} redox reactions retards the charge/discharge rates of LMFP[16]. As a result, completing the Mn^{3+}/Mn^{2+} redox reactions, especially at the end of charging, is challenging. Notably, equimolar amounts of $LiMn_{0.5}Fe_{0.5}PO_4$ (1-y value of 0.5) frequently exhibit a rapid one-phase transition throughout the cycling process[48]. However, in the range of $0.5 < 1\text{-}y \leq 0.8$, LMFP inevitably undergoes a sluggish first-order two-phase transition of Mn^{3+}/Mn^{2+} redox reactions during cycling due to the inhomogeneous distribution of Mn and Fe. Unlike equimolar LMFP, this inhomogeneity can induce abrupt lattice changes in the olivine structure, accelerating kinetic degradation in LMFP cells[68,69]. With respect to Mn and Fe homogeneity in LMFP, liquid-phase synthesis methods are considered more advantageous than solid-state counterparts, despite the complexities involved in mass production. Representative methods include hydrothermal/solvothermal[15,20,23,48,52,56,58,59,61,63,67], co-precipitation[13,34,43,51,64,68], and sol-gel processes[70].

Consequently, when designing LMFP cathodes for practical applications, it is imperative to balance Li-ion transport kinetics and energy density. This balance is influenced by factors such as chemical composition, particle morphology, and atomic distribution uniformity.

Integrating advanced LMFP with compatible anodes

The compatibility and performance of LMFP cathodes with anodes for LIBs have been primarily studied using graphite and LTO, focusing on their electrochemical behavior in LMFP/graphite and LMFP/LTO full cells. Some studies have reported alternative LMFP full cells incorporating ceramic metal oxides or metallic alloys as anode materials. However, these cells demonstrated low operating voltages, poor anode utilization, and inadequate capacity retention due to anode degradation caused by large volume changes during cycling. Despite its exceptionally high specific gravimetric capacity (4,200 mA h g^{-1}), Si has not been considered an anode material for LMFP full cells. This exclusion is primarily due to challenges in controlling anode

loading and N/P ratio for proper cell balancing, as the specific capacity of Si significantly exceeds that of LMFP. The components and key electrochemical performances of the reported LMFP full cells are summarized in Table 2, providing a comprehensive overview of their characteristics.

As demonstrated in Table 2, the combination of the LMFP composition, anode type, and window voltage collectively determines the operating voltage, reversible/irreversible capacity, and cycle life of LMFP full cells. In addition to the anode materials, enhancing the structural integrity of the LMFP is crucial to prevent the dissolution of Mn^{2+} ions into the electrolyte. These ions migrate to the anode surface, degrading SEI layers and causing irreversible capacity loss[71]. Furthermore, parasitic reactions induced by metal reduction within the SEI layer generate undesirable gases. In contrast to LTO, which lacks SEI layers and exhibits lower surface reactivity, graphite anodes with thick SEI layers are particularly susceptible to these issues [Figure 6]. Therefore, the stability of the SEI layer against metal reduction reactions is intrinsically linked to the electrical performance and thermal stability of graphite anodes. To maintain a stable SEI layer on the graphite surface, even at elevated temperatures (e.g., 60 °C) or high voltages, effective strategies include incorporating electrolyte additives (e.g., LiDFOB and LiFSI) and applying surface coatings (e.g., LFP)[70,72-74]. Another strategy involves pre-lithiating the LMFP half cells before assembling them into LMFP full cells[42]. This approach compensates for irreversible Li loss during initial SEI formation and mitigates side reactions in full cells during cycling, thereby enhancing overall performance and stability.

LTO offers a constant reversible capacity (155-160 mA h g^{-1}) and high coulombic efficiency (~100%) during cycling, making it highly advantageous for the reliable design of LMFP full cells. Compared to full cells containing NCM and/or graphite, LMFP/LTO exhibits superior thermal stability and safety due to their low specific heat evolution in both lithiated and delithiated states[75,76].

CONCLUSION AND OUTLOOK

Advancements in LIBs require cathode materials with higher energy density and superior thermal stability, which surpass the performance of commercially validated layered NCM and olivine LFP. LMFP is particularly important, as its energy density is at least 10% higher than that of LFP while maintaining comparable structural and thermal stability. Furthermore, LMFP demonstrates excellent electrochemical compatibility with NCM due to their similar voltage windows. Currently, battery manufacturers employ proprietary Mn/Fe ratios (e.g., $LiMn_{0.6}Fe_{0.4}PO_4$ and $LiMn_{0.7}Fe_{0.3}PO_4$) and various production processes (e.g., carbothermal reduction, hydrothermal/solvothermal, co-precipitation, and sol-gel) for LMFP, with the primary applications focusing on blending it with NCM to enhance stability and reduce costs.

The independent use of LMFP as a cathode material can be realized only if the complex effects of its Mn/Fe ratio, particle size, antisite defects, charge/discharge rates, and compositional uniformity on charge/discharge cycling and capacity decay mechanisms are fully understood. Therefore, predicting changes in the one- or two-phase transition regions of the Mn^{3+}/Mn^{2+} and Fe^{3+}/Fe^{2+} redox reactions during cycling for any LMFP composition remains challenging. This issue is critical when designing optimal LMFP cathode materials. Increasing the Mn content (1-y) in LMFP leads to an increase in energy density, driven by the expansion of the high-voltage Mn^{3+}/Mn^{2+} redox region. Conversely, the structural stability and cycling performance of LMFP are compromised by intensified Jahn-Teller distortion and Mn dissolution, both of which result from the high concentration of Mn^{3+} ions. Additionally, the sluggish Mn^{3+}/Mn^{2+} redox reactions, accompanied by two-phase nucleation/growth transitions, deteriorate the kinetics of LMFP at higher Mn contents. Meanwhile, reducing particle size and achieving uniform Fe and Mn distribution can expand the metastable single-phase transition region for the Mn^{3+}/Mn^{2+} and Fe^{3+}/Fe^{2+} redox reactions during cycling. Therefore, developing appropriate synthesis methods that can control defect chemistry and particle

Table 2. Comparison of electrochemical performances of reported LMFP full cells

LMFP composition	Window voltage (V)	Cell capacity (mA h g^{-1}@C-rate)	Capacity retention (%@cycles)	Initial coulombic efficiency (%)	Temp. (°C)	Ref.
LMFP/graphite full cells						
$LiMn_{0.67}Fe_{0.33}PO_4$	2.5-4.3	116@0.05C	-	72.5	60	[32]
-	2.0-4.3	- @0.1C	72.5@200	85	25	[33]
$LiMn_{0.85}Fe_{0.15}PO_4$	2.7-4.4	130@0.5C	85@300	93	25	[34]
$LiMn_{0.8}Fe_{0.2}PO_4$	2.7-4.25	132@0.5C	89@450	86	25	[35]
$LiMn_{0.63}Fe_{0.37}PO_4$	2.5-4.4	115@1C	85@50	97.5	20	[36]
$LiMn_{0.6}Fe_{0.4}PO_4$	-	110@1C	78.4@500	98	25	[42]
$LiMn_{0.5}Fe_{0.5}PO_4$	2.5-4.3	95@0.5C	95@300	-	25	[43]
$LiMn_{0.8}Fe_{0.2}PO_4$	2.5-4.2	-	90@100	-	55	[60]
$LiMn_{0.8}Fe_{0.2}PO_4$	2.0-4.25	130@0.5C	79@100	-	30	[71]
$LiMn_{0.8}Fe_{0.2}PO_4$	2.0-4.25	130@0.5C	66@100	-	60	[71]
LMFP/LTO full cells						
$LiMn_{0.8}Fe_{0.2}PO_4$	1.7-2.7	150@0.1C	-	89	25	[44]
$LiMn_{0.8}Fe_{0.2}PO_4$	0.8-2.7	153@0.5C	96@100	90	30	[46]
$LiMn_{0.8}Fe_{0.2}PO_4$	0.8-2.7	150@0.5C	52@100	-	60	[46]
$LiMn_{0.5}Fe_{0.5}PO_4$	0.8-2.7	147@0.1C	-	95.6	25	[48]
$LiMn_{0.5}Fe_{0.5}PO_4$	0.8-2.7	134@1C	92.5@500	100	25	[48]
$LiMn_{0.8}Fe_{0.2}PO_4$	1.0-3.0	70@0.1C	92@200	95	25	[49]
$LiMn_{0.5}Fe_{0.5}PO_4$	0.5-3.0	141@1C	-	96	25	[50]
$LiMn_{0.8}Fe_{0.2}PO_4$	0.8-2.9	141@1C	76.6@100	97	25	[51]
$LiMn_{0.5}Fe_{0.5}PO_4$	0.5-3.0	144@1C	74.3@120	95.5	25	[52]
Alternative LMFP full cells						
$LiMn_{0.8}Fe_{0.2}PO_4$	0.5-3.75	85@0.2	94@30	85	25	[55]
$LiMn_{0.8}Fe_{0.2}PO_4$	0.5-3.75	130@0.12	80@10	92	25	[56]
$LiMn_{0.5}Fe_{0.5}PO_4$	1.6-4.2	100@0.2C	-	95	25	[57]

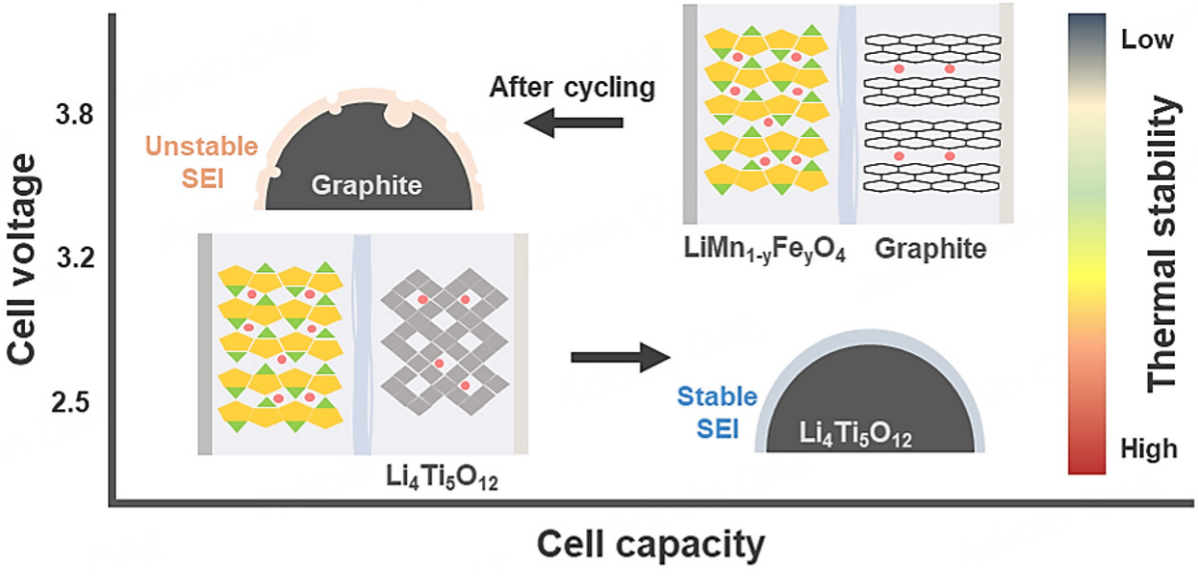

Figure 6. Summary and comparison of LMFP/graphite and LMFP/LTO full cells with respect to capacity, voltage, and thermal stability.

size of LMFP is highly recommended. It is essential to carefully balance particle size and packing density for practical applications.

From an electrode perspective, improving the adhesion between the active materials, conductive agents, and current collectors is essential for prolonging the lifespan of LMFP cells. One effective approach is to dry LMFP electrodes at temperatures above the melting point of the PVDF binder. Graphite and LTO are promising anode materials for LMFP full cells. In LMFP/graphite full cells, migrated Mn^{2+} ions from the LMFP cathode can disrupt the SEI layers on the surface of the graphite anode, leading to gas evolution due to undesirable side reactions. Therefore, surface protection of both LMFP and graphite particles, along with pre-lithiation of the graphite anode, should be implemented. Limiting the upper voltage window of LMFP/graphite full cells is also desirable to minimize the negative effects of Mn^{3+}/Mn^{2+} reactions and electrolyte decomposition at high SOC. In terms of thermal and cycling stabilities, coupling an LMFP cathode with an LTO anode holds considerable promise. The lower capacity and higher electrode potential of LTO compared to graphite are not critical for load-leveling applications, where space limitations are less of a concern.

Given the significant advancements in LFP cathode materials, which have been widely adopted in the battery industry, LMFP is anticipated to emerge as a mainstream cathode material for future LIBs due to its enhanced performance. To realize this potential, further precise studies are required to understand the intrinsic characteristics of LMFP cathode materials with and without cycling, investigate the internal phenomena occurring within the LMFP full cell during operation at varying temperatures, and optimize different cell parameters.

DECLARATIONS

Author's contributions

Writing - original draft: Jung, H.; Park, J. H.
Data curation: Oh, C.; Park, S.
Investigation: An, S.; Bang, J.
Visualization: Youn, J.; Lee, J.
Funding acquisition: Jung, H.
Writing - review & editing, project administration: Han, D.

Availability of data and materials

Not applicable.

Financial support and sponsorship

This work was supported by the Technology Innovation Program Development Program (RS-2024-00445441, Development of 8 mAh/cm^2 large-area electrode technology for high-capacity all-solid-state batteries) funded By the Ministry of Trade, Industry & Energy(MOTIE, Korea).

Conflicts of interest

All authors declared that there are no conflicts of interest.

Ethical approval and consent to participate

Not applicable.

Consent for publication

Not applicable.

REFERENCES

1. Winter, M.; Barnett, B.; Xu, K. Before Li ion batteries. *Chem. Rev.* **2018**, *118*, 11433-56. DOI PubMed
2. Goodenough, J. B.; Park, K. S. The Li-ion rechargeable battery: a perspective. *J. Am. Chem. Soc.* **2013**, *135*, 1167-76. DOI PubMed
3. Zhang, B.; Wang, X.; Wang, S.; et al. High-energy-density lithium manganese iron phosphate for lithium-ion batteries: progresses, challenges, and prospects. *J. Energy. Chem.* **2025**, *100*, 1-17. DOI
4. Chung, S. Y.; Bloking, J. T.; Chiang, Y. M. Electronically conductive phospho-olivines as lithium storage electrodes. *Nat. Mater.* **2002**, *1*, 123-8. DOI PubMed
5. Qiu, Z.; Man, Q.; Mu, Y.; et al. Modification strategies for enhancing the performance of lithium manganese iron phosphate cathodes in lithium-ion batteries. *Chem. Methods.* **2025**, 2400065. DOI
6. Nekahi, A.; Kumar, A. M. R.; Li, X.; Deng, S.; Zaghib, K. Sustainable $LiFePO_4$ and $LiMn_xFe_{1-x}PO_4$ (x=0.1-1) cathode materials for lithium-ion batteries: a systematic review from mine to chassis. *Mater. Sci. Eng. R.* **2024**, *159*, 100797. DOI
7. Yang, L.; Deng, W.; Xu, W.; et al. Olivine $LiMn_xFe_{1-x}PO_4$ cathode materials for lithium ion batteries: restricted factors of rate performances. *J. Mater. Chem. A.* **2021**, *9*, 14214-32. DOI
8. Shiozaki, M.; Yamashita, H.; Hirayama, Y.; Ogami, T.; Kanamura, K. Blending lithium nickel manganese cobalt oxide with lithium iron manganese phosphate as cathode materials for lithium-ion batteries with enhanced electrochemical performance. *Electrochemistry* **2023**, *91*, 077007. DOI
9. Kobayashi, G.; Yamada, A.; Nishimura, S. I.; et al. Shift of redox potential and kinetics in $Li_x(Mn_yFe_{1-y})PO_4$. *J. Power. Sources.* **2009**, *189*, 397-401. DOI
10. Yamada, A.; Kudo, Y.; Liu, K. Y. Phase diagram of $Li_x(Mn_yFe_{1-y})PO_4$ ($0 \le x, y \le 1$). *J. Electrochem. Soc.* **2001**, *148*, A1153. DOI
11. Loftager, S.; Schougaard, S. B.; Vegge, T.; García-Lastra, J. M. Density functional theory study of redox potential shifts in $Li_xMn_yFe_{1-y}PO_4$ battery electrodes. *J. Phys. Chem. C.* **2019**, *123*, 102-9. DOI
12. Di Lecce, D.; Brescia, R.; Scarpellini, A.; Prato, M.; Hassoun, J. A high voltage olivine cathode for application in lithium-ion batteries. *ChemSusChem* **2016**, *9*, 223-30. DOI
13. Sun, Y. K.; Oh, S. M.; Park, H. K.; Scrosati, B. Micrometer-sized, nanoporous, high-volumetric-capacity $LiMn_{0.85}Fe_{0.15}PO_4$ cathode material for rechargeable lithium-ion batteries. *Adv. Mater.* **2011**, *23*, 5050-4. DOI PubMed
14. Xu, E.; Sun, X.; Lyv, W.; et al. Optimizing the electrochemical performance of olivine $LiMn_xFe_{1-x}PO_4$ cathode materials: ongoing progresses and challenges. *Ind. Eng. Chem. Res.* **2024**, *63*, 9631-60. DOI
15. Hu, Q.; Wang, L.; Han, G.; et al. Revealing the voltage decay of $LiMn_{0.7}Fe_{0.3}PO_4$ cathodes over cycling. *Nano. Energy.* **2024**, *123*, 109422. DOI
16. Li, S.; Zhang, H.; Liu, Y.; Wang, L.; He, X. Comprehensive understanding of structure transition in $LiMn_yFe_{1-y}PO_4$ during delithiation/lithiation. *Adv. Funct. Mater.* **2024**, *34*, 2310057. DOI
17. Ravnsbæk, D. B.; Xiang, K.; Xing, W.; et al. Engineering the transformation strain in $LiMn_yFe_{1-y}PO_4$ olivines for ultrahigh rate battery cathodes. *Nano. Lett.* **2016**, *16*, 2375-80. DOI
18. Zhang, Y.; Gao, Z.; Su, Z. A novel strategy for preparing nano-sized and high-performance $LiMn_xFe_{1-x}PO_4$ cathode materials from discarded $LiMn_2O_4$ and $LiFePO_4$. *Energy. Technol.* **2024**, *12*, 2301277. DOI
19. Jiang, X.; Li, L.; Wang, X.; Luo, Z. Concentration-gradient structural $LiFe_{0.5}Mn_{0.5}PO_4$/C prepared via co-precipitation reaction for advanced lithium-ion batteries. *Chemphyschem* **2024**, *25*, e202300930. DOI
20. Xie, L.; Cui, J.; Ma, Y.; et al. Microsphere $LiMn_{0.6}Fe_{0.4}PO_4$/C cathode with unique rod-like secondary architecture for high energy lithium ion batteries. *Chem. Eng. J.* **2024**, *499*, 156513. DOI
21. Sun, K.; Luo, S. H.; Wang, G.; et al. Fine structure and electrochemical performance investigations of spherical $LiMn_{0.6}Fe_{0.4}PO_4$/C cathode material synthesized via a spray-drying route at various calcination temperatures. *Langmuir* **2024**, *40*, 16571-81. DOI
22. Yao, M.; Wang, Y. T.; Chen, J. A.; et al. Mn-rich induced alteration on band gap and cycling stability properties of $LiMn_xFe_{1-x}PO_4$ cathode materials. *ACS. Appl. Mater. Interfaces.* **2024**, *16*, 66077-88. DOI
23. Zoller, F.; Böhm, D.; Luxa, J.; et al. Freestanding $LiFe_{0.2}Mn_{0.8}PO_4$/rGO nanocomposites as high energy density fast charging cathodes for lithium-ion batteries. *Mater. Today. Energy.* **2020**, *16*, 100416. DOI
24. Hu, Q.; Liao, J.; Xiao, X.; et al. Ultrahigh rate capability of manganese based olivine cathodes enabled by interfacial electron transport enhancement. *Nano. Energy.* **2022**, *104*, 107895. DOI
25. Zhang, B.; Meng, W.; Gong, Y.; et al. [001]-oriented $LiMn_{0.6}Fe_{0.4}PO_4$/C nanorod microspheres contributing high-rate performance to olivine-structured cathode for lithium-ion battery. *Mater. Today. Energy.* **2022**, *30*, 101162. DOI
26. Peng, L.; Zhang, X.; Fang, Z.; et al. General facet-controlled synthesis of single-crystalline {010}-oriented $LiMPO_4$ (M = Mn, Fe, Co) nanosheets. *Chem. Mater.* **2017**, *29*, 10526-33. DOI

27. Hwang, W.; Kim, J.; Kim, S.; et al. Unveiling olivine cathodes for high energy-density lithium-ion batteries: a comprehensive review from the atomic level to the electrode scale. *J. Mater. Chem. A.* **2024**, *12*, 27800-24. DOI
28. Deng, Y.; Yang, C.; Zou, K.; Qin, X.; Zhao, Z.; Chen, G. Recent advances of Mn-rich $LiFe_{1-y}Mn_yPO_4$ ($0.5 \leq y < 1.0$) cathode materials for high energy density lithium ion batteries. *Adv. Energy. Mater.* **2017**, *7*, 1601958. DOI
29. Sun, K.; Luo, S. H.; Du, N.; Wei, Y.; Yan, S. Research progress of lithium manganese iron phosphate cathode materials: from preparation to modification. *Electroanalysis* **2024**, *36*, e202400120. DOI
30. Balogun, M. S.; Qiu, W.; Luo, Y.; et al. A review of the development of full cell lithium-ion batteries: the impact of nanostructured anode materials. *Nano. Res.* **2016**, *9*, 2823-51. DOI
31. Martha, S. K.; Grinblat, J.; Haik, O.; et al. $LiMn_{0.8}Fe_{0.2}PO_4$: an advanced cathode material for rechargeable lithium batteries. *Angew. Chem. Int. Ed.* **2009**, *48*, 8559-63. DOI
32. Guéguen, A.; Castro, L.; Dedryvère, R.; et al. The electrode/electrolyte reactivity of $LiFe_{0.33}Mn_{0.67}PO_4$ compared to $LiFePO_4$. *J. Electrochem. Soc.* **2013**, *160*, A387-93. DOI
33. Starke, B.; Seidlmayer, S.; Schulz, M.; et al. Gas evolution and capacity fading in $LiFe_xMn_{1-x}PO_4$/graphite cells studied by neutron imaging and neutron induced prompt gamma activation analysis. *J. Electrochem. Soc.* **2017**, *164*, A3943-8. DOI
34. Oh, S. M.; Myung, S. T.; Park, J. B.; Scrosati, B.; Amine, K.; Sun, Y. K. Double-structured $LiMn_{0.85}Fe_{0.15}PO_4$ coordinated with $LiFePO_4$ for rechargeable lithium batteries. *Angew. Chem. Int. Ed.* **2012**, *51*, 1853-6. DOI
35. Theivanayagam, M. G.; Hu, T.; Ziebarth, R.; et al. Improvement in hydrophobicity of olivine lithium manganese iron phosphate cathodes by SiF_4 treatment for lithium-ion batteries. *Solid. State. Ion.* **2015**, *281*, 82-8. DOI
36. Ehteshami, N.; Eguia-Barrio, A.; de Meatza, I.; Porcher, W.; Paillard, E. Adiponitrile-based electrolytes for high voltage, graphite-based Li-ion battery. *J. Power. Sources.* **2018**, *397*, 52-8. DOI
37. Lv, Z.; Li, M.; Lin, J.; et al. First-principles study on $LiMn_{0.5}Fe_{0.5}PO_4$ doping to decrease the Jahn-Teller effect. *J. Solid. State. Electrochem.* **2024**, *28*, 577-87. DOI
38. Li, Z.; You, Y.; Zhu, Z.; et al. Surface iron concentration gradient: a strategy to suppress Mn^{3+} Jahn-Teller effect in lithium manganese iron phosphate. *Appl. Surf. Sci.* **2025**, *682*, 161689. DOI
39. Zhao, X.; An, L.; Sun, J.; Liang, G. $LiNi_{0.5}Co_{0.2}Mn_{0.3}O_2$-$LiMn_{0.6}Fe_{0.4}PO_4$ mixture with both excellent electrochemical performance and low cost as cathode material for power lithium ion batteries. *J. Electrochem. Soc.* **2018**, *165*, A142-8. DOI
40. Lei, P.; Wei, Y.; Xiong, Y.; et al. Capacity degradation prediction model of $LiMn_{0.6}Fe_{0.4}PO_4$/$LiNi_{0.5}Co_{0.2}Mn_{0.3}O_2$ composite cathode materials for lithium-ion batteries. *Ionics* **2025**, *31*, 217-28. DOI
41. Xiao, J.; Xiong, Y.; Lei, P.; et al. A dual kalman filtering algorithm for estimating the SOC of lithium-ion batteries with $LiMn_{0.6}Fe_{0.4}PO_4$/$LiNi_{0.5}Co_{0.2}Mn_{0.3}O_2$ cathode based on multi-innovation and schmidt orthogonal transformation. *J. Electrochem. Soc.* **2023**, *170*, 090514. DOI
42. Wu, Y.; Ju, J.; Shen, B.; et al. Rich-carbonyl carbon catalysis facilitating the Li_2CO_3 decomposition for cathode lithium compensation agent. *Small* **2024**, *20*, e2311891. DOI
43. Vanaphuti, P.; Manthiram, A. Enhancing the Mn redox kinetics of $LiMn_{0.5}Fe_{0.5}PO_4$ cathodes through a synergistic co-doping with niobium and magnesium for lithium-ion batteries. *Small* **2024**, *20*, e2404878. DOI
44. Martha, S. K.; Haik, O.; Borgel, V.; et al. $Li_4Ti_5O_{12}$/$LiMnPO_4$ lithium-ion battery systems for load leveling application. *J. Electrochem. Soc.* **2011**, *158*, A790. DOI
45. Xu, G.; Han, P.; Dong, S.; Liu, H.; Cui, G.; Chen, L. $Li_4Ti_5O_{12}$-based energy conversion and storage systems: status and prospects. *Coord. Chem. Rev.* **2017**, *343*, 139-84. DOI
46. Borgel, V.; Gershinsky, G.; Hu, T.; Theivanayagam, M. G.; Aurbach, D. $LiMn_{0.8}Fe_{0.2}PO_4$/$Li_4Ti_5O_{12}$, a possible Li-ion battery system for load-leveling application. *J. Electrochem. Soc.* **2013**, *160*, A650-7. DOI
47. Jalkanen, K.; Vuorilehto, K. Entropy change characteristics of $LiMn_{0.67}Fe_{0.33}PO_4$ and $Li_4Ti_5O_{12}$ electrode materials. *J. Power. Sources.* **2015**, *273*, 351-9. DOI
48. Yang, J.; Li, C.; Guang, T.; et al. Zero lithium miscibility gap enables high-rate equimolar $Li(Mn,Fe)PO_4$ solid solution. *Nano. Lett.* **2021**, *21*, 5091-7. DOI
49. Zou, Q. Q.; Zhu, G. N.; Xia, Y. Y. Preparation of carbon-coated $LiFe_{0.2}Mn_{0.8}PO_4$ cathode material and its application in a novel battery with $Li_4Ti_5O_{12}$ anode. *J. Power. Sources.* **2012**, *206*, 222-9. DOI
50. Yang, C. C.; Hwu, H. J.; Lin, S. J.; Chien, W. C.; Shih, J. Y. Preparation of high-rate performance $Li_4Ti_5O_{12}$/C anode material in $Li_4Ti_5O_{12}$/$LiFe_{0.5}Mn_{0.5}PO_4$ batteries. *Electrochim. Acta.* **2014**, *125*, 637-45. DOI
51. Li, J.; Wang, Y.; Wu, J.; Zhao, H.; Liu, H. CNT-embedded $LiMn_{0.8}Fe_{0.2}PO_4$/C microsphere cathode with high rate capability and cycling stability for lithium ion batteries. *J. Alloys. Compd.* **2018**, *731*, 864-72. DOI
52. Yu, M.; Li, J.; Ning, X. Improving electrochemical performance of $LiMn_{0.5}Fe_{0.5}PO_4$ cathode by hybrid coating of Li_3VO_4 and carbon. *Electrochim. Acta.* **2021**, *368*, 137597. DOI
53. Daigle, J. C.; Rochon, S.; Asakawa, Y.; et al. High performance $LiMnFePO_4$/$Li_4Ti_5O_{12}$ full cells by functionalized polymeric additives. *Mater. Adv.* **2021**, *2*, 253-60. DOI
54. Yang, C. C.; Hung, Y. W.; Lue, S. J. Improved electrochemical properties of $LiFe_{0.5}Mn_{0.5}PO_4$/C composite materials via a surface coating process. *J. Power. Sources.* **2016**, *325*, 565-74. DOI
55. Hariharan, S.; Ramar, V.; Joshi, S. P.; Balaya, P. Developing a light weight lithium ion battery - an effective material and electrode design for high performance conversion anodes. *RSC. Adv.* **2013**, *3*, 6386. DOI

56. Hariharan, S.; Saravanan, K.; Ramar, V.; Balaya, P. A rationally designed dual role anode material for lithium-ion and sodium-ion batteries: case study of eco-friendly Fe_3O_4. *Phys. Chem. Chem. Phys.* **2013**, *15*, 2945-53. DOI PubMed
57. Di Lecce, D.; Fasciani, C.; Scrosati, B.; Hassoun, J. A Gel-polymer Sn-C/$LiMn_{0.5}Fe_{0.5}PO_4$ battery using a fluorine-free salt. *ACS. Appl. Mater. Interfaces.* **2015**, *7*, 21198-207. DOI
58. Di Lecce, D.; Verrelli, R.; Hassoun, J. New lithium ion batteries exploiting conversion/alloying anode and $LiFe_{0.25}Mn_{0.5}Co_{0.25}PO_4$ olivine cathode. *Electrochim. Acta.* **2016**, *220*, 384-90. DOI
59. Yu, H.; Zhang, E.; Yu, J.; et al. Relaxing the Jahn-Teller distortion of $LiMn_{0.6}Fe_{0.4}PO_4$ cathodes via Mg/Ni dual-doping for high-rate and long-life Li-ion batteries. *J. Mater. Chem. A.* **2024**, *12*, 26076-82. DOI
60. Leslie, K.; Harlow, J.; Rathore, D.; Tuul, K.; Metzger, M. Correlating Mn dissolution and capacity fade in $LiMn_{0.8}Fe_{0.2}PO_4$/graphite cells during cycling and storage at elevated temperature. *J. Electrochem. Soc.* **2024**, *171*, 040520. DOI
61. Meng, Y.; Wang, Y.; Zhang, Z.; Chen, X.; Guo, Y.; Xiao, D. A phytic acid derived $LiMn_{0.5}Fe_{0.5}PO_4$/Carbon composite of high energy density for lithium rechargeable batteries. *Sci. Rep.* **2019**, *9*, 6665. DOI PubMed PMC
62. Song, Y.; Zhong, H.; Hu, T.; et al. Dually encapsulated $LiMn_{0.6}Fe_{0.4}PO_4$ architecture with MXenes and amorphous carbon to achieve high-performance and ultra-stable lithium batteries. *J. Mater. Chem. A.* **2025**, *13*, 2590-9. DOI
63. Hu, H.; Liu, X.; Lei, Y.; et al. Enhancing the ultra-high rate capability of manganese-based olivine cathode by in situ catalytic growth of graphene carbon layer. *J. Energy. Storage.* **2024**, *79*, 110198. DOI
64. Wang, Y.; Yong, F.; Wang, Z.; et al. $LiMn_{0.8}Fe_{0.2}PO_4$/C nanoparticles via polystyrene template carburizing enhance the rate capability and capacity reversibility of cathode materials. *ACS. Appl. Nano. Mater.* **2024**, *7*, 4024-34. DOI
65. Han, D. W.; Ryu, W. H.; Kim, W. K.; et al. Tailoring crystal structure and morphology of $LiFePO_4$/C cathode materials synthesized by heterogeneous growth on nanostructured $LiFePO_4$ seed crystals. *ACS. Appl. Mater. Interfaces.* **2013**, *5*, 1342-7. DOI
66. Ravnsbæk, D. B.; Xiang, K.; Xing, W.; et al. Extended solid solutions and coherent transformations in nanoscale olivine cathodes. *Nano. Lett.* **2014**, *14*, 1484-91. DOI
67. Guo, X.; Wang, M.; Huang, X.; Zhao, P.; Liu, X.; Che, R. Direct evidence of antisite defects in $LiFe_{0.5}Mn_{0.5}PO_4$ via atomic-level HAADF-EELS. *J. Mater. Chem. A.* **2013**, *1*, 8775. DOI
68. Amisse, R.; Hamelet, S.; Hanzel, D.; Courty, M.; Dominko, R.; Masquelier, C. Nonstochiometry in $LiFe_{0.5}Mn_{0.5}PO_4$: structural and electrochemical properties. *J. Electrochem. Soc.* **2013**, *160*, A1446-50. DOI
69. Burgos, A.; Du, J.; Yan, D.; et al. Off-stoichiometric design of a manganese-rich mixed olivine Li-ion cathode for improved specific energy. *Mater. Today. Energy.* **2024**, *45*, 101658. DOI
70. Zhao, Q.; Li, X.; Tang, F.; et al. Compatibility between Lithium bis(oxalate)borate-based electrolytes and a $LiFe_{0.6}Mn_{0.4}PO_4$/C cathode for lithium-ion batteries. *Energy. Technol.* **2017**, *5*, 406-13. DOI
71. Ziv, B.; Borgel, V.; Aurbach, D.; Kim, J. H.; Xiao, X.; Powell, B. R. Investigation of the reasons for capacity fading in Li-ion battery cells. *J. Electrochem. Soc.* **2014**, *161*, A1672. DOI
72. Liu, Y.; Wen, X.; Huang, T.; Yu, A. Electrochemically induced interface by LiBOB to enhance cycling performance of $LiFe_{0.4}Mn_{0.6}PO_4$ cathode for lithium-ion batteries. *J. Power. Sources.* **2024**, *623*, 235398. DOI
73. Fang, G.; Pan, Y.; Yang, H.; Chen, W.; Wu, M. Enhanced $LiMn_{0.8}Fe_{0.2}PO_4$ cathode performance enabled by the 1,3,2-dioxathiolane-2,2-dioxide electrolyte additive. *J. Phys. Chem. C.* **2024**, *128*, 6877-86. DOI
74. Li, S.; Tang, R.; Hu, C.; Niu, X.; Wang, L. Potassium 2-thienyl tri-fluoroborate as a functional electrolyte additive enables stable interfaces for Li/$LiFe_{0.3}Mn_{0.7}PO_4$ batteries. *J. Colloid. Interface. Sci.* **2023**, *646*, 150-8. DOI
75. Jeong, S. Y.; Lee, S.; Lee, H.; et al. Thermal characteristics of $LiMn_xFe_{1-x}PO_4$ (x = 0, 0.6) cathode materials for safe lithium-ion batteries. *J. Power. Sources.* **2025**, *626*, 235755. DOI
76. Park, J. S.; Oh, S. M.; Sun, Y. K.; Myung, S. T. Thermal properties of fully delithiated olivines. *J. Power. Sources.* **2014**, *256*, 479-84. DOI